A low-noise differential microphone inspired by the ears of the parasitoid fly *Ormia ochracea*

R. N. Miles, Q. Su, W. Cui, and M. Shetye
Department of Mechanical Engineering, State University of New York, P.O. Box 6000, Binghamton, New York 13902-6000

F. L. Degertekin, B. Bicen, and C. Garcia
G. W. Woodruff School of Mechanical Engineering, Georgia Institute of Technology, 801 Ferst Drive Northwest, Atlanta, Georgia 30332-0405

S. Jones
Department of Mechanical Engineering, State University of New York, P.O. Box 6000, Binghamton, New York 13902-6000

N. Hall
G. W. Woodruff School of Mechanical Engineering, Georgia Institute of Technology, 801 Ferst Drive Northwest, Atlanta, Georgia 30332-0405

A miniature differential microphone is described having a low-noise floor. The sensitivity of a differential microphone suffers as the distance between the two pressure sensing locations decreases, resulting in an increase in the input sound pressure-referred noise floor. In the microphone described here, both the diaphragm thermal noise and the electronic noise are minimized by a combination of novel diaphragm design and the use of low-noise optical sensing that has been integrated into the microphone package. The differential microphone diaphragm measures 1×2 mm^2 and is fabricated out of polycrystalline silicon. The diaphragm design is based on the coupled directionally sensitive ears of the fly *Ormia ochracea*. The sound pressure input-referred noise floor of this miniature differential microphone has been measured to be less than 36 dBA. © *2009 Acoustical Society of America.* [DOI: 10.1121/1.3082118]

I. INTRODUCTION

Any pressure-sensitive microphone that has an output that depends on the direction of a propagating sound wave must detect the difference in acoustic pressure at a minimum of two points in space. While directional microphones have been used in audio applications for many decades, they can be very challenging to design for applications that have substantial size constraints. One important application for miniature directional microphones is in hearing aids. It is well-known that the use of directional acoustic sensing in hearing aids can be a very effective means of reducing the influence of unwanted background acoustic noise and as a result can significantly improve the understanding of speech in noisy environments (Amlani *et al.*, 2006; Blamey *et al.*, 2006; Hornsby and Ricketts, 2007; Ricketts *et al.*, 2003; Walden *et al.*, 2004). In hearing aids, it is highly desirable that the distance between the points at which the pressure is sensed be kept to a bare minimum, on the order of a few millimeters in order for the size of the device to be cosmetically acceptable. Unfortunately, as this separation distance is reduced, the difference in the sensed pressures is also reduced proportionally. In miniature directional microphones, the desired pressure difference signal can be similar in level to the internal noise and can be very difficult to accurately extract from the average, or common-mode pressure. The main purpose of the present study is to describe a miniature differential microphone that is able to accurately detect pressure differences with minimal influence of microphone noise.

A. Biological inspiration

The approach to the design of the differential microphone described here is based on the mechanical principles employed in the ears of the fly *Ormia ochracea* (Miles *et al.,* 1995). This fly detects spatial gradients in the sound pressure because it has a mechanical connection between the tympana, resulting in the two ears moving in opposite directions in response to pressure differences on their outer surfaces. This differs from the detection of pressure differences by simply allowing the incident sound to drive either side of a single membrane or by subtracting the outputs of two non-directional microphones. It is well-known that by combining the detection of the pressure gradient along with the pressure, it is straightforward to construct an output that has any of a number of first-order directivity patterns (Olson, 1947; Beranek, 1954). The essence of the mechanical response of *Ormia*'s ears has been shown to be a mechanical realization of a simple sum and difference circuit invented by Blumlein in the earliest days of stereo audio (Blumlein, 1931; Gerzon, 1994; Miles *et al.*, 1997). A simple system to mimic this is described in Miles *et al.* (1997). The mechanical connection between the *Ormia*'s ears has been shown to dramatically

improve the accuracy of estimates of sound source orientation by an analysis of the Cramer–Rao bound (Akcakaya and Nehorai, 2008).

While there are a number of remarkable characteristics of *Ormia*'s auditory system, the feature that the present study focuses on is the fly's unusual apparatus for detecting sound pressure gradients. This is driven by the fact that accurately detecting pressure gradients is the greatest challenge in creating miniature directional microphones. *Ormia*'s ears respond to a combination of the pressure gradient and the pressure to produce directionally sensitive tympanal response (Miles *et al.*, 1995). Achieving the proper combination of the responses due to pressure and pressure gradient is remarkable in a biological system but in a man-made device, it is a simple matter to combine these signals by either an analog circuit or digital processor.

In *Ormia ochracea*'s auditory system, it has been shown that the mechanical structure of the ears allows the response to pressure gradient and pressure to combine in such a way that the tympanum that is closest to a sound source responds with 10–20 dB greater amplitude than the opposite tympanum. This enhanced response amplitude causes the neural sensory cells in the ear closest to the sound source to fire with dramatically less latency than those of the opposite ear (Oshinsky, 1998; Mason *et al.*, 2001). The reduced latency of the neural response provides the central nervous system with the essential information on the orientation of the sound source.

The auditory system of *Ormia ochracea* thus amounts to a multi-stage processor to indicate the direction of a sound source. Because the two tympana are so close together that temporal cues in the incident sound wave are not usable by the nervous system, the mechanical structure of the ears acts to convert these miniscule time of arrival differences into significant differences in tympanal displacements. These differences in displacement are then converted by the sensory nervous system into significantly enhanced temporal differences in neural response, which are then much more readily processed by the central nervous system. The end result for the central nervous system is essentially the expansion or amplification of temporal cues in the incident sound.

Again, the focus of the present effort is to borrow ideas from the fly to help solve the challenging problem in creating miniature directional microphones: the detection of sound pressure gradients.

B. Detection of pressure gradients

The typical method of creating a directional sound sensor is to use a pair of closely spaced nondirectional microphones, as is commonly employed in directional hearing aids. In the absence of microphone noise and mismatches in phase or amplitude sensitivity of the two microphones, it is possible to determine the direction of arrival of a sound relative to the line connecting the microphones with arbitrary accuracy with this first-order small aperture array. Unfortunately, for microphone spacings that are very small relative to the sound wavelength, microphone noise and mismatches in sensitivity or phase can adversely affect the directional

response. The primary difficulty is that for small microphone spacings it is difficult to accurately detect differences in the pressures incident on the two microphones. The focus of the present effort is to create a small sensor that provides an accurate measure of the pressure gradient without suffering from these problems.

Any pressure-sensitive diaphragm is a differential sensor because it responds to the difference in pressure on its two sides. Great care is typically taken to convert it to a nondirectional microphone by designing an enclosure to prevent sound from driving one of the two sides of the diaphragm. While a pressure difference sensor is simple to create, the challenge is to obtain adequate response when the size of the device is reduced. Low sensitivity to the desired signal results in a greater influence of electronic and mechanical/thermal noise. In a system that is intended to localize sound, the Cramer–Rao bound on the accuracy of the localization is strongly determined by the system noise floor (see, for example, Friedlander, 1984). In a first-order sound localization system that relies on processing of a combination of the first-order pressure gradient and the pressure [as is done in *Ormia*'s ears (Miles *et al.*, 1997)], the challenge then is to obtain an accurate, low-noise measurement of the pressure gradient; the pressure itself can be measured with much less difficulty because it is much higher in level than the pressure gradient.

The system used for detection of pressure gradients in *Ormia's* ears suggests an alternative method of constructing a differential microphone than the use of a simple single diaphragm. A primary aim of the present study is to examine whether or not this approach can result in a differential microphone having better noise performance than can be achieved with existing approaches. The noise performance of a microphone is strongly dependent on its size. In the case of a differential microphone, the noise performance also strongly depends on the effective distance between the points of pressure measurement. In the following, we have attempted to take these two critical features into account.

C. Other studies of *Ormia*-inspired microphones

A number of researchers have reported the construction of microphones based on the ears of *O. ochracea*. A system is described in Miles *et al.* (1997) that combines the outputs of two nondirectional microphones in a manner that is analogous to the in-phase and out-of-phase vibrational modes of *Ormia's* coupled ears, which provide measures of the pressure and pressure gradient, respectively. This use of the combination of the average and differential pressures to achieve a directionally-sensitive output, as mentioned above, is described in Blumlein (1931). Microphone diaphragms having a directional response based on *Ormia's* ears, using the combination of these two modes of vibration, are described in Yoo *et al.* (2002). The diaphragms were fabricated out of either polycrystalline silicon or Parylene. The diaphragms had dimensions of 1×2 mm^2 and had thicknesses of 1.2 and 2.4 μm for the polysilicon and Parylene diaphragms, respectively. The design and analysis of the acoustic response of these microphones is described in Gibbons and Miles (2000).

Ormia-inspired differential microphone diaphragms are described in Miles *et al.* (2002) having improved sensitivity over those of the earlier design of Gibbons and Miles (2000) and Yoo *et al.* (2002). Measured frequency responses are shown to be in excellent agreement with predictions of the response to incident sound. The microphone diaphragms again had dimensions of 1×2 mm^2 and were fabricated out of polycrystalline silicon. These diaphragms have also been described in Miles *et al.* (2004) and Miles and Hoy (2006) and are predecessors of the design described in the present study. Saito *et al.* (2002) reported a microphone diaphragm inspired by *Ormia's* ears that is supported on a gimbal. This circular diaphragm is made of bronze and has a radius of 10.8 mm and a thickness of 30 μm. A signal processing scheme, intended to be used with a miniature, silicon version of this diaphragm to achieve two-dimensional sound source separation is described in Ono *et al.* (2005).

An *Ormia*-inspired differential microphone having dimensions of 1×2 mm^2, fabricated out of polysilicon and that incorporates optical sensing to obtain an electronic output, was reported by Cui *et al.* (2006). The electronic output of the microphone is shown to have a directivity pattern similar to the figure-eight pattern expected for a first-order differential microphone. A CMOS-compatible directional microphone inspired by *Ormia's* ears is presented in Sung *et al.* (2007). The diaphragm dimensions are 840×410 μm^2. The acoustic response of the diaphragm was detected using a laser vibrometer and was shown to have a directivity pattern similar to the expected figure eight. A pair of mylar diaphragms having radii of 3.5 mm and 22 μm thickness that are glued to a 2.54 cm $\times$ 1.2 mm $\times$ 100 μm rod made of either steel or brass to mimic *Ormia's* ears has been reported by Chen and Yu (2008). It is shown that the incorporation of the connecting rod increased the time delay of the acoustic response of the two diaphragms.

It should also be pointed out that *Ormia's* ability to localize sound has inspired a number of researchers to develop signal processing algorithms for sound source localization that utilize the detection of sound pressure gradients in air (see, for example, Ando, 1995; Stanacevic and Cauwenberghs, 2005; Lockwood and Jones, 2006; Ando *et al.*, 2007; and Mohan *et al.*, 2008).

The differential microphone diaphragm described here is designed to behave like a rigid plate that is supported on carefully-designed flexible pivots (Miles *et al.*, 2004). Pressure gradients acting on the exposed surface of the diaphragm produce a net moment and hence cause it to rotate about its central hinge supports. By taking advantage of microfabrication technology, the diaphragm can be designed to be very lightweight and have very high compliance, enabling it to respond well to minute sound pressure gradients even though the largest dimension of the differential diaphragm is only 2 mm.

D. Optical sensing

In order to transduce the motion of the diaphragm into an electronic signal, we have incorporated a high-sensitivity, low-noise optical sensing scheme providing minimum de-

tectable displacement on the order of 10 fm/$\sqrt{\text{Hz}}$, using approximately 61 μW of laser power (Hall and Degertekin, 2002; Lee *et al.*, 2004; Cui *et al.*, 2006; Miles and Degertekin, 2007). The majority of successful miniature microphone designs employ capacitive sensing, which suffers from instability when used on highly compliant diaphragms because the required bias voltage causes a significant force that attracts the diaphragm toward the biasing electrode. The use of low-noise optical sensing allows our differential microphone diaphragm to have very high compliance, which is important in achieving good sensitivity to pressure gradients.

The use of optical sensing and a highly compliant and responsive diaphragm has resulted in the achievement of very low electronic noise from the microphone. As a result, the noise floor of the microphone is primarily influenced by its thermal noise, resulting from random impacts between the diaphragm and the surrounding air. It is well-known that the equivalent input sound pressure associated with this thermal noise is proportional to the amount of passive energy dissipation in the system (Gabrielson, 1993; Thompson *et al.*, 2002; Hall *et al.*, 2007). The design developed here does not require the use of a backplate electrode, which is typically the dominant cause of viscous damping in capacitive microphones (Thompson *et al.*, 2002; Homentcovschi and Miles, 2004; Homentcovschi and Miles, 2005; Hall *et al.*, 2007). In addition, because the dominant motion of the diaphragm consists of rotation about its flexible supports, acoustic radiation damping and other sources of viscous damping can be kept to a minimum. As a result, the overall design approach leads to a system having low noise relative to the desired pressure gradient being sensed.

In the following, the designs of the microphone diaphragm and the optical sensing scheme are described along with an analysis of the noise performance. The microphone's response and noise outputs are shown to agree very well with predictions. Finally, the noise floor of the differential microphone is compared with what can be achieved with current, commercially available hearing aid microphones.

II. DIFFERENTIAL MICROPHONE DIAPHRAGM AND OPTICAL SENSOR

Figure 1 shows a design model of the microphone diaphragm. It consists of a stiffened plate supported by flexible pivots. The overall dimensions of the diaphragm are 1×2 mm^2. The diaphragm is fabricated out of polycrystalline silicon having a thickness of approximately 1 μm. Stiffeners, indicated in Fig. 1, are incorporated to cause the diaphragm to respond as a rigid plate that is supported on flexible pivots. The stiffeners are approximately 20 μm tall and 2 μm thick. The finite element design model has been used in a numerical optimization procedure to optimize the dimensions of the diaphragm and the stiffeners to achieve low noise and high acoustic sensitivity. Approximate expressions are used for the noise performance and the sensitivity (as derived below), which are used to construct an objective function in the iterative design. The ANSYS finite element model accounts for all of the resonant vibrational modes that can have an influence on the acoustic response. The struc-
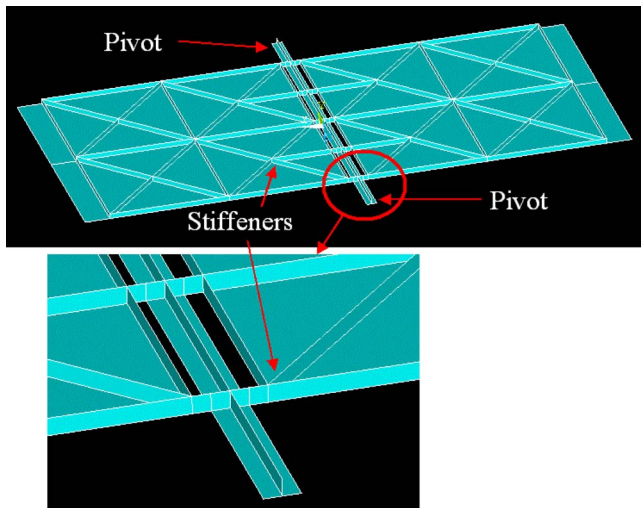
FIG. 1. (Color online) Design model of the microphone diaphragm. The diaphragm consists of a stiffened plate that is supported by flexible pivots. The stiffeners are also indicated in Fig. 4.

tural optimization has been carried out to ensure that the response is dominated by the mode in which the diaphragm rotates about its supports as a rigid plate. The dimensions of the stiffeners have been optimized to attenuate the influence of these undesirable modes. The mode shapes predicted by the design model are shown in Fig. 2. The first mode, consisting of out-of-phase motion of the two ends of the diaphragm, has a predicted resonant frequency of 821.7 Hz while the second mode, having both ends move in-phase, has a predicted resonant frequency of 15 002.7 Hz. The stiffening effect of the air volume within the package behind the microphone diaphragm has been taken into account in the
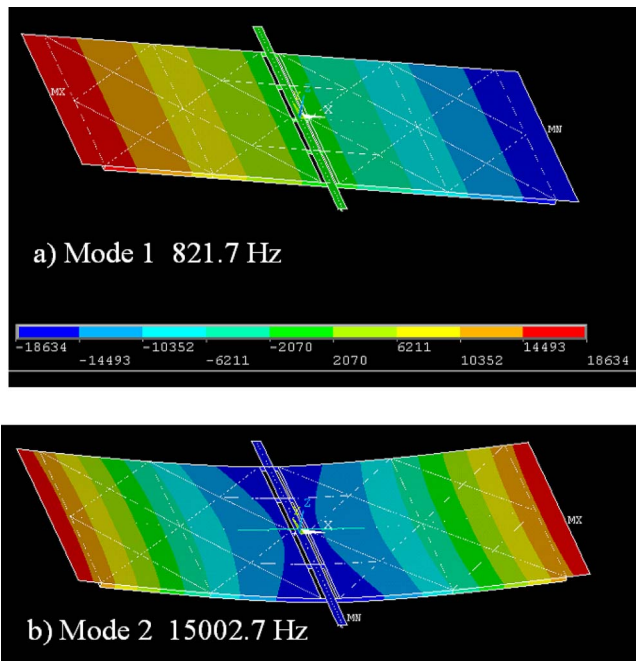

FIG. 2. (Color online) The mode shapes of the first two resonant modes of the diaphragm as predicted by the finite element (ANSYS) design model. The first mode shown in panel (a) consists of the diaphragm rotating as a rigid plate about its supporting pivots. The second mode shown in panel (b) consists of both ends of the diaphragm moving in-phase.
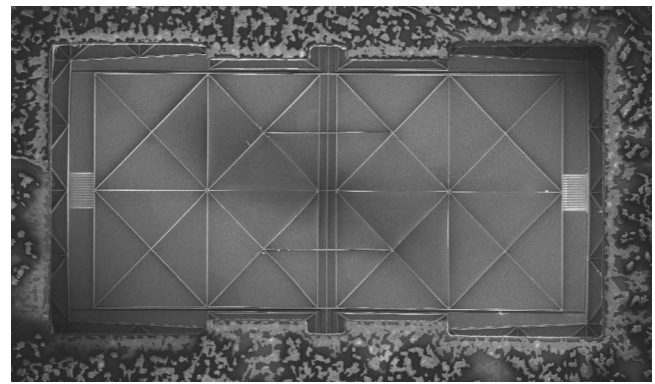

FIG. 3. Scanning electron micrograph of the microphone diaphragm. This image shows the back side of the diaphragm through the hole etched through the back of the wafer.

finite element model. Figure 3 shows a scanning electron micrograph showing the stiffeners as seen through a hole that has been etched through the thickness of the silicon wafer, as described below. Figures 4(a) and 4(b) show a photograph and the mask design of the top surface of the microphone diaphragm. The figure shows gold mirrors at each end of the diaphragm used in the optical sensing system described below.

Figure 5 shows the fabrication process flow for the microphone diaphragm. The fabrication starts with a deep reactive ion trench etch into the 4 in. test grade silicon wafer that acts as the mold for the polysilicon stiffeners. This is followed by a wet oxidation at 1100 °C to grow a 1 μm thick thermal oxide layer on the wafer surface and in the trenches [Fig. 5(a)]. This oxide is used as an etch stop for a subsequent backside cavity etch. The next step is to deposit and planarize polycrystalline silicon to form a 1 μm thick diaphragm having stiffeners. The phosphorus-doped polysilicon is deposited at 580 °C and subsequently annealed at 1100 °C in argon gas for 60 min in order to reduce intrinsic stress in the film. The polysilicon is then etched to define the optical grating and the slits that separate the diaphragm from
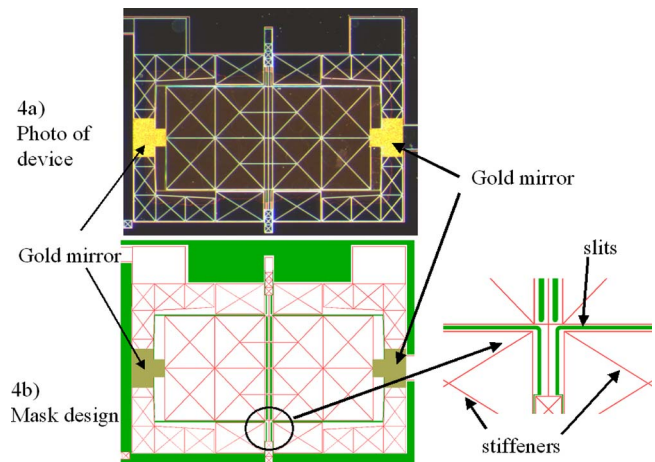

FIG. 4. (Color online) Photograph (a) and the mask design (b) of the top surface of the microphone diaphragm. The figure shows gold mirrors at each end of the diaphragm used in the optical sensing system. A close-up of the mask design is shown to indicate the stiffeners and the slit that is cut to form the perimeter of the diaphragm.
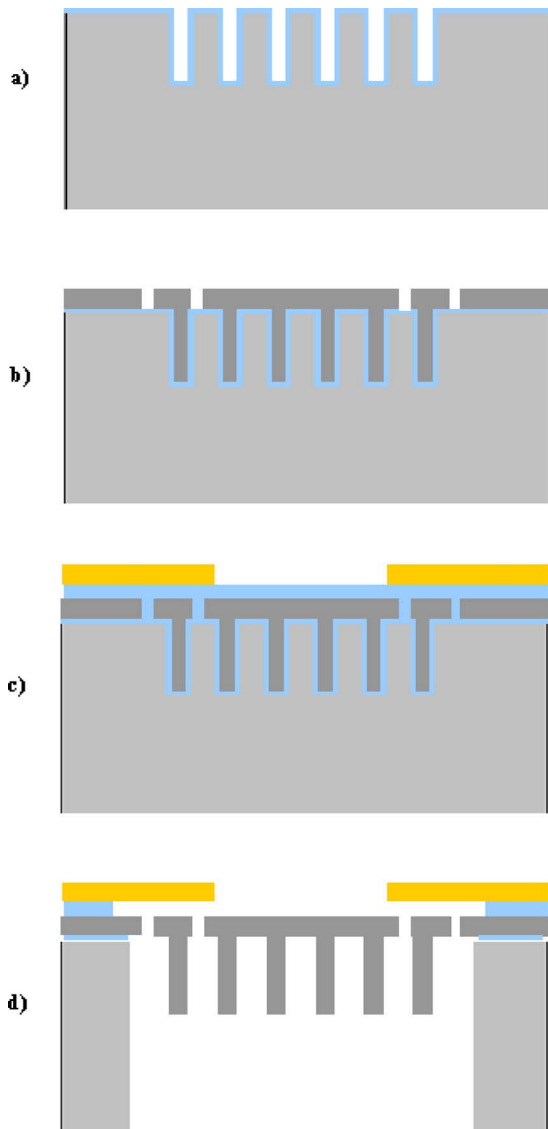
FIG. 5. (Color online) Fabrication process flow for the microphone diaphragm. The fabrication starts with a deep reactive ion trench etch into the 4-in. test grade silicon wafer. This is followed by a wet oxidation to grow a 1 μm thick thermal oxide layer on the wafer surface and in the trenches [Fig. 5(a)]. The next step is to deposit and planarize polycrystalline silicon to form a 1 μm thick diaphragm having stiffeners. The polysilicon is then etched to define the optical grating and the slits that separate the diaphragm from the substrate [Fig. 5(b) and in the inset of Fig. 4(b)]. This is followed by PECVD oxide deposition, chrome and gold seed layer evaporation, and gold plating to form the gold mirrors [Fig. 5(c)]. The back cavity is then etched using a deep reactive ion etch and the thermal and PECVD oxide layers are removed in buffered oxide etchant to release the structures [Fig. 5(d)].

the substrate [Fig. 5(b)]. This is followed by plasma enhanced chemical vapor deposition (PECVD) oxide deposition, chrome and gold seed layer evaporation, and gold plating to form the gold mirrors. Both the oxide layer and the gold mirrors are 5 μm in thickness [Fig. 5(c)]. The back cavity is then etched using a deep reactive ion etch and the thermal and PECVD oxide layers are removed in buffered oxide etchant to release the structures [Fig. 5(d)].

A schematic of the optical sensing scheme is shown in Fig. 6 (Cui *et al.*, 2006; Miles and Degertekin, 2007). This consists of an optical grating (an array of slits), a mirror
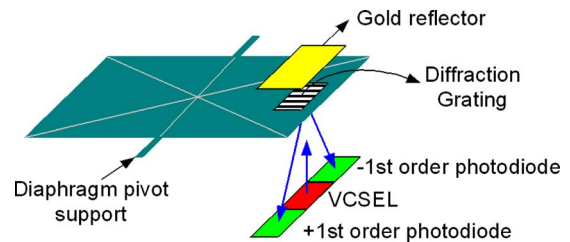

FIG. 6. (Color online) Schematic of the differential microphone diaphragm and the optical components. This consists of an optical grating (an array of slits), a mirror placed above the diaphragm, a light source (in this case a VCSEL), and photodetectors. The light that is reflected back to the photodetectors is modulated by the relative motion between the grating on the diaphragm and the mirror. The electrical output of the photodetectors is thus proportional to the diaphragm motion, providing the sensitivity of an interferometer.

placed above the diaphragm, a light source [in this case a vertical cavity surface emitting laser (VCSEL)], and photodetectors. The light that is reflected back to the photodetectors is modulated by the relative motion between the grating on the diaphragm and the mirror. The electrical output of the photodetectors is thus proportional to the diaphragm motion, providing the sensitivity of an interferometer. Similar optical detection structures have already been used to implement low-noise micromachined omnidirectional microphones (Hall *et al.*, 2005; 2007). Figure 7 shows an end-view of the diaphragm and optical components. The optical components and the silicon chip containing the microphone diaphragm have been assembled in a package depicted in Figs. 8 and 9. The silicon chip containing the directional microphone diaphragm shown in Figs. 8 and 9 contains an array of three microphone diaphragms, two differential diaphragms, and one nondirectional microphone diaphragm. This microphone array on the chip has been fabricated in order to explore the use of co-located directional microphones in a signal processing scheme as part of this effort described in Mohan *et al.* (2008).

In Sec. III, we examine the physical principles that determine the noise performance of the microphone. Experimental results will then be described and compared with predictions.

III. ANALYTICAL MODEL FOR MICROPHONE RESPONSE AND NOISE FLOOR

In order to construct a simplified model that can predict the microphone's noise performance, it is necessary to write down expressions for the response to sound. Because the
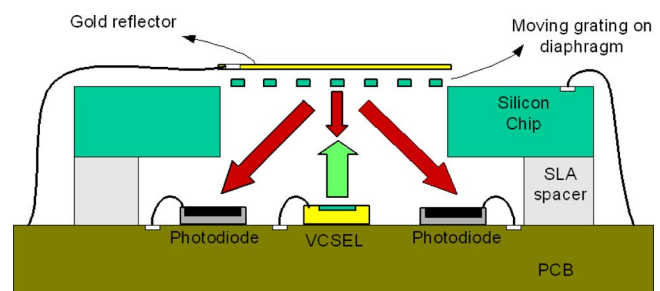

FIG. 7. (Color online) End-view of the diaphragm and optical components.

J. Acoust. Soc. Am., Vol. 125, No. 4, April 2009

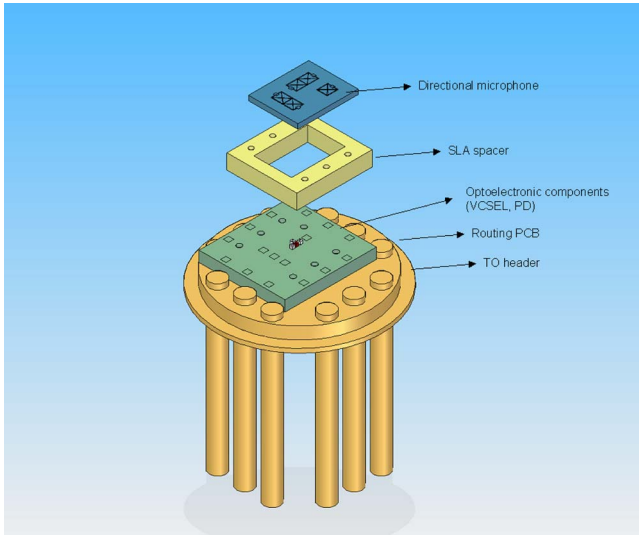Miles *et al.*: Low noise differential microphone   2017

FIG. 8. (Color online) Package assembly design for the optical components and the silicon chip containing the microphone diaphragm.

diaphragm is intended to rotate about its hinge axis due to the sound pressure gradient, we first write the relation between the pressure gradient and the applied moment about the axis of rotation. A simple lumped-parameter model for the diaphragm's rotation can then be written in terms of the equivalent mass moment of inertia, I, about the axis of rotation, the equivalent torsional stiffness, k_t, and the equivalent viscous damping constant, c_t. The equivalent driving moment due to thermal excitation is then determined along with the equivalent pressure of an incident plane sound wave that would cause the same response as the thermal excitation. While the microphone diaphragm has been designed to respond primarily in its first resonant mode, the second mode of vibration, in which the two ends translate in-phase, can influence the response. The effects of the response of this translational mode along with the noise due to electronic circuits are included in an expression for the equivalent sound pressure noise.
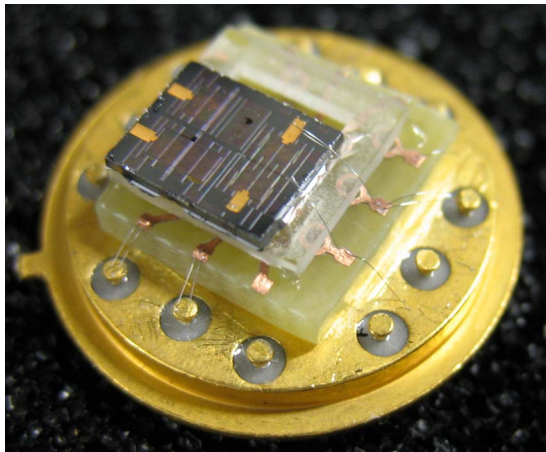

FIG. 9. (Color online) Photograph of the assembled microphone. The optical components are below the microphone diaphragm chip and are not visible.

A. Relation between sound pressure gradient and driving moment

We will assume that the microphone diaphragm is small relative to the wavelength of sound so that the spatial variation in pressure is small over its surface. Taking the origin of our coordinate system to be at the center of the diaphragm with the rotation oriented in the y direction and the length L measured in the x direction, the sound pressure as a function of x and t can be expanded in a two-term Taylor's series,

$$p(x,t) \approx p(0,t) + x \left. \frac{\partial p}{\partial x} \right|_{x=0}. \tag{1}$$

The moment applied by the sound field about the diaphragm's axis of rotation is then given by

$$M(t) = \int_{-L/2}^{L/2} bxp(x,t)dx \approx \int_{-L/2}^{L/2} bxp(0,t)dx$$
$$+ \int_{-L/2}^{L/2} bx^2 \left. \frac{\partial p}{\partial x} \right|_{x=0} dx, \tag{2}$$

where we have used the expansion in Eq. (1). b is the width of the diaphragm. Carrying out the integrations on the right in Eq. (2) gives

$$M(t) \approx \left. \frac{\partial p}{\partial x} \right|_{x=0} I_A, \tag{3}$$

where, for this simple rectangular diaphragm, the area moment of inertia about the axis of rotation is $I_A = bL^3/12$.

Equation (3) shows that the moment applied to the diaphragm is the product of the pressure gradient in the x direction and the area moment of inertia.

As mentioned above, the diaphragm has been designed so that the only vibrational modes that influence its motion in the audible frequency range have one of the two mode shapes shown in Fig. 2. While additional, ultrasonic modes could easily be included in our noise analysis, our present aim is to construct a model containing only the essential features that guide design.

B. Lumped-parameter model for diaphragm rotation

We first consider the motion due to the mode which is dominated by rotation about the pivot axis. Then, the contribution to the noise due to the second mode of vibration will be accounted for. Since the diaphragm has been designed so that its dominant vibrational mode consists of pure rotation as a rigid body, the equation of motion of the diaphragm in terms of its rotation, θ, may be taken to be

$$I\ddot{\theta} + k_t\theta + c_t\dot{\theta} = M(t), \tag{4}$$

where I is the mass moment of inertia, k_t is the equivalent torsional stiffness, and c_t is the effective dashpot constant for rotation. Equation (4) can also be expressed in the more convenient form

$$\ddot{\theta} + \omega_0^2\theta + 2\omega_0\zeta\dot{\theta} = \frac{M(t)}{I}, \tag{5}$$

where $\omega_0^2 = k_t/I$, and ζ is the damping ratio, $\zeta = c_t/2\sqrt{k_tI}$.

Because our aim is to examine the response of the diaphragm due to random thermal excitation from the surrounding medium, and compare that to the response due to sound, the incident sound field will be taken to be a weakly stationary random signal. This enables us to examine the effects of both the acoustic and thermal excitations using power spectral densities. By using Eq. (5), the power spectral density of the rotation of the diaphragm can be shown to be

$$S_{\theta\theta}(\omega) = \frac{S_{MM}(\omega)/I^2}{(\omega_0^2 - \omega^2)^2 + (2\omega_0\zeta\omega)^2}, \quad (6)$$

where $S_{MM}(\omega)$ is the power spectral density of the applied moment, $M(t)$.

C. Response due to thermal excitation

We would like to compare the response of the microphone due to acoustic excitation with that due to random thermal excitation from the surrounding gas. The equipartition theorem and the Nyquist relation can be used to calculate the response due to thermal excitation. Assuming, for now, that the response is dominated by a single rotational mode of vibration as assumed above, then

$$\tfrac{1}{2}K_BT = \tfrac{1}{2}k_tE[\theta^2]_n, \quad (7)$$

where $K_B = 1.38 \times 10^{-23}$ J/K is Boltzmann's constant, and T is the absolute temperature. $E[\theta^2]_n$ is the mean square response due to the thermal excitation. If the power spectral density of the moment due to thermal excitation, S_{MM}^N, is independent of frequency, ω, then for a system governed by Eq. (5), the mean square response of the rotation is obtained by integrating the power spectral density of Eq. (6) over all frequencies (Lin, 1967),

$$E[\theta^2]_n = \frac{\pi S_{MM}^N}{2\zeta\omega_0^3 I^2} = \frac{\pi S_{MM}^N}{k_tc_t} = \frac{K_BT}{k_t}, \quad (8)$$

where we have also used Eq. (7). Equation (8) then gives the two-sided power spectral density of the applied moment due to the thermal excitation (with units of $(\text{N m})^2/\text{rad/s}$),

$$S_{MM}^N = \frac{K_BTc_t}{\pi}. \quad (9)$$

D. Equivalent input pressure due to a plane sound wave

Since directional microphones are typically characterized in terms of their response to incident plane waves, it is convenient to re-cast Eq. (9) to determine the equivalent sound pressure of an incident wave that would correspond to the response due to thermal excitation. If the sound pressure is due to a plane wave incident with a speed c_0 at an angle ϕ relative to the direction that is tangent to the plane of the diaphragm, then the pressure on the diaphragm can be expressed as

$$p(x,t) = p\left(t - \frac{x}{c_0}\cos(\phi)\right). \quad (10)$$

In the case where the sound pressure is a weakly stationary random signal, the power spectral density of the sound pressure at $x=0$ may be obtained from the Fourier transform of the autocorrelation function of the pressure, $R_{pp}(\tau) = E[p(t)p(t-\tau)]$, where E denotes the expected value,

$$S_{pp}(\omega) = \frac{1}{2\pi}\int_{-\infty}^{\infty} e^{-j\omega\tau}R_{pp}(\tau)d\tau. \quad (11)$$

Since the moment, $M(t)$, in Eq. (3) depends on the pressure gradient, we need the power spectral density of the gradient to determine the power spectral density of the response. From Eq. (10), the gradient of the pressure, $dp/dx = p_x(x,t)$ at $x=0$ is

$$p_x(t) = \dot{p}(t)\frac{-\cos(\phi)}{c_0}. \quad (12)$$

The autocorrelation function of the gradient, $\partial p/\partial x$ at $x=0$, may then be written as

$$R_{p_xp_x}(\tau) = E[p_x(t)p_x(t-\tau)] = \left(\frac{\cos(\phi)}{c_0}\right)^2 E[\dot{p}(t)\dot{p}(t-\tau)]. \quad (13)$$

Taking the transform of Eq. (13) as in Eq. (11) enables us to obtain the power spectral density of the pressure gradient as

$$S_{p_xp_x}(\omega) = \left(\frac{\omega\cos(\phi)}{c_0}\right)^2 S_{pp}(\omega). \quad (14)$$

By using Eqs. (3) and (14), we can obtain the relation between the power spectral density of the applied moment and that of the pressure for this plane wave,

$$S_{MM}(\omega) = I_A^2\left(\frac{\omega\cos(\phi)}{c_0}\right)^2 S_{pp}(\omega). \quad (15)$$

Equations (6) and (15) give the power spectrum of the response as

$$S_{\theta\theta}(\omega) = \frac{(\omega\cos(\phi)/c_0)^2(I_A/I)^2 S_{pp}(\omega)}{(\omega_0^2 - \omega^2)^2 + (2\omega_0\omega\zeta)^2}. \quad (16)$$

The relation between the spectral densities in Eq. (15) along with Eq. (9) can allow us to write the power spectral density of the pressure due to a plane wave, $S_{pp}(\omega)$, that would cause the same response as the thermal excitation,

$$S_{pp}^N(\omega) = \frac{S_{MM}^N}{I_A^2(\omega\cos(\phi)/c_0)^2} = \frac{K_BTc_t}{\pi I_A^2(\omega\cos(\phi)/c_0)^2}. \quad (17)$$

This result is normally evaluated for sound that is incident at $\phi=0$, the most sensitive direction. The power spectrum of the response due to thermal excitation may be written by replacing $S_{pp}(\omega)$ with $S_{pp}^N(\omega)$ in Eq. (16),

J. Acoust. Soc. Am., Vol. 125, No. 4, April 2009

Miles *et al.*: Low noise differential microphone   2019

$$S_{\theta\theta}^N(\omega) = \frac{(\omega\cos(\phi)/c_0)^2(I_A/I)^2 S_{pp}^N(\omega)}{(\omega_0^2 - \omega^2)^2 + (2\omega_0\omega\zeta)^2}$$

$$= \frac{K_B T c_t/(\pi I^2)}{(\omega_0^2 - \omega^2)^2 + (2\omega_0\omega\zeta)^2}. \qquad (18)$$

E. Influence of the translational mode on noise performance

While the motion of the diaphragm is typically dominated by rotation, θ, at most frequencies of interest in audio applications, it is also important to account for the second mode shown in Fig. 2(b) in which the ends of the diaphragm move in the direction normal to the plane. This translational mode will be described by the coordinate $X(t)$. Assuming that the properties of the diaphragm are symmetric about its axis of rotation, the coordinates $X(t)$ and $\theta(t)$ will be uncoupled. The equation governing $X(t)$ is

$$m\ddot{X} + kX + c\dot{X} = p(0,t)A,$$

$$\ddot{X} + \omega_X^2 X + 2\omega_X\zeta_X\dot{X} = p(0,t)A/m, \qquad (19)$$

where m is the effective mass, k is the equivalent stiffness, c is the equivalent dashpot constant, ω_X is the natural frequency, and ζ_X is the damping ratio. A is the equivalent area of the diaphragm and $p(0,t)$ is the surface average of the sound pressure acting on the diaphragm [which is also equal to $p(x,t)$ at $x=0$].

As in Eq. (6), the power spectral density of the translational mode is related to that of the acoustic pressure by

$$S_{XX}(\omega) = \frac{S_{pp}(\omega)(A/m)^2}{(\omega_X^2 - \omega^2)^2 + (2\omega_X\zeta_X\omega)^2}. \qquad (20)$$

If both the rotational and translational modes are accounted for, the equipartition theorem states that each uncoupled mode receives the same thermal energy, $K_B T/2$, so that the thermal energy imparted to the translational mode is

$$\tfrac{1}{2}K_B T = \tfrac{1}{2}kE[X^2]_N, \qquad (21)$$

where $E[X^2]_N$ is the mean square of the response of the mode due to thermal excitation. Proceeding as in Eqs. (5), (6), and (18), the power spectral density of the translational mode due to thermal excitation is

$$S_{XX}^N(\omega) = \frac{K_B T c/(\pi m^2)}{(\omega_X^2 - \omega^2)^2 + (2\omega_X\omega\zeta_X)^2}. \qquad (22)$$

Because the response is detected at the end of the diaphragm at a distance d from the pivot, the detected displacement, $W(t)$, is related to the translation and rotation by

$$W(t) = X(t) + d\theta(t). \qquad (23)$$

F. Equivalent input pressure noise including effects of electronic circuit noise

Since the output of the microphone must be detected using non-ideal electronic circuits, there will be some contribution to the noise due to noise generated in the circuits. This

electronic noise can be represented by an equivalent displacement noise of the diaphragm $W^e(t)$, having a power spectral density given by $S_{WW}^{Ne}(\omega)$. The noise due to the electronics is not examined in detail here; the relative contribution due to laser intensity noise, shot noise in the photodetectors, and noise from other electronic components will be examined in other studies.

Since the thermal excitation is comprised of spatially random impacts of gas molecules with the diaphragm, the electronic noise and the thermal responses of the two modes are uncorrelated. Equations (18), (22), and (23) allow us to write the power spectral density of the thermal response of $W(t)$ as

$$S_{WW}^N(\omega) = \frac{K_B T c_t d^2/(\pi I^2)}{(\omega_0^2 - \omega^2)^2 + (2\omega_0\omega\zeta)^2}$$

$$+ \frac{K_B T c/(\pi m^2)}{(\omega_X^2 - \omega^2)^2 + (2\omega_X\omega\zeta_X)^2} + S_{WW}^{Ne}(\omega). \qquad (24)$$

Having the power spectral density of the equivalent displacement noise in Eq. (24), it is possible to estimate the power spectral density of the sound pressure that would produce this level of noise. To compute this input pressure-referred spectral density, note that the power spectral density of the displacement response due to sound pressure is

$$S_{WW}(\omega) = |H_{PW}(\omega)|^2 S_{pp}(\omega), \qquad (25)$$

where

$$H_{PW}(\omega) = \frac{A/m}{\omega_X^2 - \omega^2 + 2\omega_X\omega\zeta_X\hat{j}} + \frac{\hat{j}\omega\cos(\phi)dI_A/(c_0 I)}{\omega_0^2 - \omega^2 + 2\omega_0\omega\zeta\hat{j}}. \qquad (26)$$

Equations (24) and (25) may be used to obtain an equivalent sound pressure power spectral density that would cause the predicted noise response power spectrum, $S_{WW}^N(\omega)$,

$$S_{pp}^{Nt}(\omega) = \left(\frac{K_B T c_t d^2/(\pi I^2)}{(\omega_0^2 - \omega^2)^2 + (2\omega_0\omega\zeta)^2} \right.$$

$$+ \frac{K_B T c/(\pi m^2)}{(\omega_X^2 - \omega^2)^2 + (2\omega_X\omega\zeta_X)^2}$$

$$\left. + S_{WW}^{Ne}(\omega) \right) \frac{1}{|H_{PW}(\omega)|^2}. \qquad (27)$$

In order to allow direct comparisons with measured results, the predicted spectral density of the displacement noise in Eq. (24) can be modified to predict the output voltage noise, $S_{VV}^N(\omega)$, by

$$S_{VV}^N(\omega) = |H_{WV}(\omega)|^2 \times S_{WW}^N(\omega), \qquad (28)$$

where $H_{WV}(\omega)$ is the transfer function between the diaphragm displacement and the output voltage in V/m, given in Table I.

Knowing the displacement relative to the pressure, $H_{PW}(\omega)$, in Eq. (26) and the output voltage for a given displacement, $H_{WV}(\omega)$, the output voltage relative to the input sound pressure is

TABLE I. Parameters used in predictions.

Estimated diaphragm mechanical parameters	
Mass moment of inertia, $I = 5 \times 10^{-15}$ kg m^2	
Rotation mode natural frequency, $f_r = 735$ Hz	
Rotational mode damping ratio, $\xi_r = 0.16$	
Rotational dashpot	
constant = $c_t = 7.389 \times 10^{-12}$ N m s/rad	
Translational mode effective mass, $m = 4 \times 10^{-8}$ kg	
Translational mode natural frequency, $f_t = 15220$ Hz	
Translational mode damping ratio, $\xi_t = 0.25$	
Translational mode dashpot	
constant = $c = 0.001\,912\,6$ N s/m	

Diaphragm dimensions
Length, $1 = 2.2 \times 10^{-3}$ m
Width, $b = 10^{-3}$ m
Area moment of inertia, $I_A = bl^3/12 = 8.87 \times 10^{-13}$ m^4

Electrical parameters
Electrical/mechanical sensitivity: $H_{WV}(f) = 0.0056$ V/nm

Parameters for noise prediction
Boltzmann's constant = $K_B = 1.38 \times 10^{-23}$ J/K
Absolute temperature = $T = 293$ K

Diaphragm parameters from ANSYS finite element design model
$I = 3.49 \times 10^{-15}$ kg m^2
Rotational mode natural frequency, $f_r = 821.7$ Hz
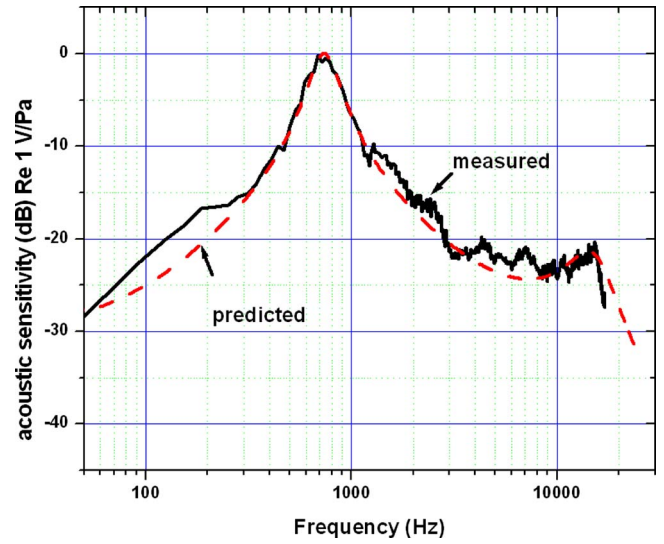Translational mode natural frequency, $f_t = 15\,002.7$ Hz

FIG. 10. (Color online) Comparison of predicted and measured electrical output in response to sound. The results are normalized relative to the sound pressure that is incident on the diaphragm. The data shown in this and the following figures were obtained by averaging auto- and/or cross power spectral density estimates from 20 records of the measured signals. The spectra were computed using the fast Fourier transform algorithm applied to the discrete time domain data. A coherence squared function was also calculated between the measured input signal and the response. Data were rejected when the coherence was less than 0.85. The coherence was typically greater than 0.95.

$$H_{PV}(\omega) = H_{PW}(\omega) \times H_{WV}(\omega). \qquad (29)$$

IV. COMPARISONS WITH EXISTING TECHNOLOGY

A straightforward and common way to create a directional acoustic sensor is through the use of a pair of omnidirectional microphones. The equivalent input-referred noise of this directional system can be estimated knowing the noise floors of the two-omnidirectional microphones, $S_{oo}^N(\omega)$, and by accounting for the loss of sensitivity to sound when the outputs of the microphones are subtracted to achieve a directional response. This loss of sensitivity can be accounted for by multiplying the output sensitivity of the omnidirectional microphones by $\omega d_o/c$, where ω is the frequency in rad/s d_o is the distance between the microphones, and c is the sound speed. In addition, because the power of the uncorrelated noise of the microphones is added when the output signals are subtracted, the resultant noise power spectrum is effectively increased by a factor of 2. By taking the difference of the two signals to achieve a directional output, the equivalent sound input-referred noise is then

$$S_{dd}^N(\omega) = 2\left(\frac{c}{\omega d_o}\right)^2 S_{oo}^N(\omega). \qquad (30)$$

To compare the equivalent input pressure noise levels of a two-omnidirectional microphone system with that of the present study, it can be more convenient to express the equivalent input noise levels in decibels. If $SPL_{oo}(\omega)$ is the equivalent input sound pressure level of the two-omnidirectional microphones, then the input-referred noise level of the directional system may be estimated from

$$SPL_{dd}(\omega) = 10 \log_{10} S_{dd}^N(\omega) = SPL_{oo}(\omega) + 3$$
$$- 20 \log_{10}\left(\frac{\omega d_o}{c}\right). \qquad (31)$$

V. MEASURED RESULTS

The electrical output of the microphone shown in Fig. 9 has been measured relative to the incident sound pressure as measured by a calibrated reference microphone. The results are shown as a function of frequency in hertz in Fig. 10 along with those predicted by Eq. (29). The sound source was oriented in the most sensitive direction for the microphone. The measured and predicted results are in very close agreement. Figure 10 shows that the frequency dependence of the sensitivity is that of a bandpass filter as expected from the form of Eq. (16) for the power spectral density of the diaphragm rotation.

Since a flat frequency response is sought in most microphone applications, it may be desirable to incorporate a compensation filter that will result in a flat frequency response over most of the audible range. This frequency compensation can be accomplished without influencing the sound input-referred noise because, as will be discussed below, the noise is dominated by the diaphragm thermal noise (and not the noise from the electronics). The diaphragm thermal noise is superimposed on the detected sound pressure so its relation to the sound pressure is not affected by subsequent process-

ing of the signal. In addition, an active electronic feedback system is being developed that provides the beneficial effects of damping for both the transient response and frequency response of the diaphragm without adversely affecting the noise performance (Miles, 2008).

The physical parameters used in evaluating Eq. (29) to obtain the predicted results shown in Fig. 10 are given in Table I. The mass moment of inertia, I, the natural frequencies, equivalent mass, m, and the damping constants have been identified empirically through a least squares curve fit of the measured displacement of the diaphragm due to sound using the method outlined in the Appendix. Table I also lists the mass moment of inertia and the first two natural frequencies predicted by our finite element design model. The predicted and measured frequencies of the rotational mode are 821.7 and 735 Hz, respectively (12% error). The predicted and measured in-phase mode frequencies are 15002.7 and 15220 Hz, respectively (1.4% error). The resonant frequencies of the fabricated device were thus very close to those of our finite element design model.

The agreement between measured and predicted results indicates that the measured characteristics of the diaphragm are consistent with those expected from an analytical model based only on the physical dimensions and known material properties. It is also important to note that the frequencies of the first two modes are separated by roughly a factor of 20, which results in the rotational mode dominating the response over a wide range of frequencies.

The relation between the output voltage and the diaphragm displacement, $H_{WV}(\omega)$ in Eqs. (28) and (29), has been obtained by measuring the electrical output and the diaphragm displacement (measured using a Veeco optical profilometer) due to a voltage applied between the mirror shown in Figs. 4, 6, and 7 and the diaphragm.

The measured directivity pattern of the diaphragm is shown in Fig. 11 along with the figure-eight pattern expected for an ideal differential microphone. The measured results are shown to be in reasonable agreement with the ideal dipole pattern.

The output noise of the microphone as predicted by Eq. (28), in terms of the single-sided power spectral density (with units of $V/\sqrt{Hz}$), is compared to the measured output noise in Fig. 12. The measurements were performed while the microphone was placed in an anechoic chamber at the Georgia Institute of Technology to minimize sources of acoustic noise. The noise floor of the anechoic chamber was measured using a 1/2 in. Larson Davis model 2541 microphone and is significantly below the measured noise shown here; external acoustic noise does not influence these results except at very low frequencies. For frequencies below about 3 kHz, the output noise is strongly influenced by the thermal noise of the rotational mode of the diaphragm as predicted by the first term in Eq. (24). As shown in Fig. 12, the total microphone noise is dominated by the thermal noise for frequencies below about 3 kHz. The discrepancy between the predicted and measured noise below 100 Hz is likely due to acoustic noise in the anechoic chamber. The discrepancy at frequencies above 3 kHz is probably due to electronic noise in the optical system.
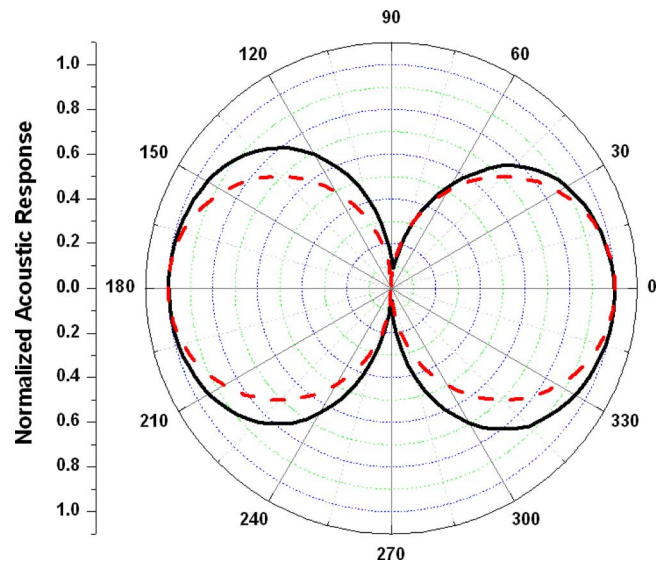

FIG. 11. (Color online) The measured directivity pattern of the diaphragm along with the figure eight pattern expected for an ideal differential microphone. The directivity measurements are performed in an anechoic chamber. The directional microphone is mounted on a rotation stage which can be controlled with a motion controller. The sound source is at a fixed location and driven by a pure tone sine wave at a frequency of approximately 800 Hz.

The equivalent sound input pressure-referred noise as predicted by Eq. (27) is compared to the measured input pressure-referred noise in Fig. 13. The measured results are obtained by dividing those of Fig. 12 by those given in Fig. 10.

The one-third octave band levels of the narrowband input pressure-referred noise of Fig. 13 are shown in Fig. 14. The corresponding dBA levels of the measured and predicted data are 35.6 and 34 dBA, respectively. The difference between the predicted and measured results is most likely due to electronic noise $S_{WW}^{Ne}(\omega)$, which has been neglected in the predictions and has not been measured independently.
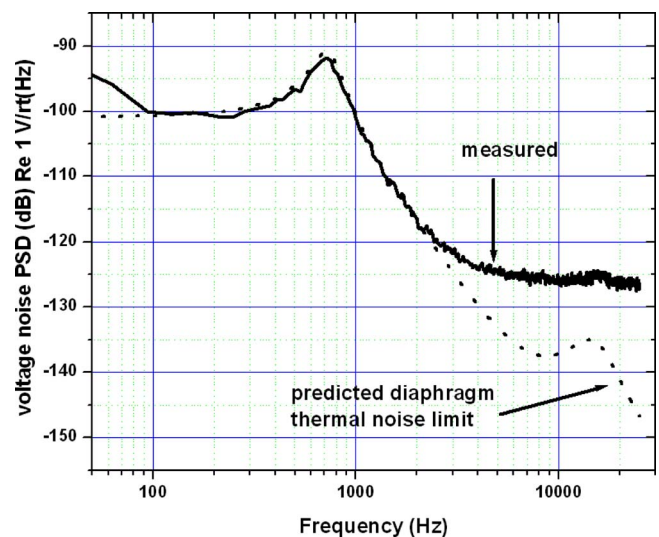

FIG. 12. (Color online) The output noise of the microphone as predicted by Eq. (28) compared to the measured output noise. The predicted results were obtained while neglecting the contribution due to the electronic noise, $S_{WW}^{Ne}(\omega)$, in Eq. (24).
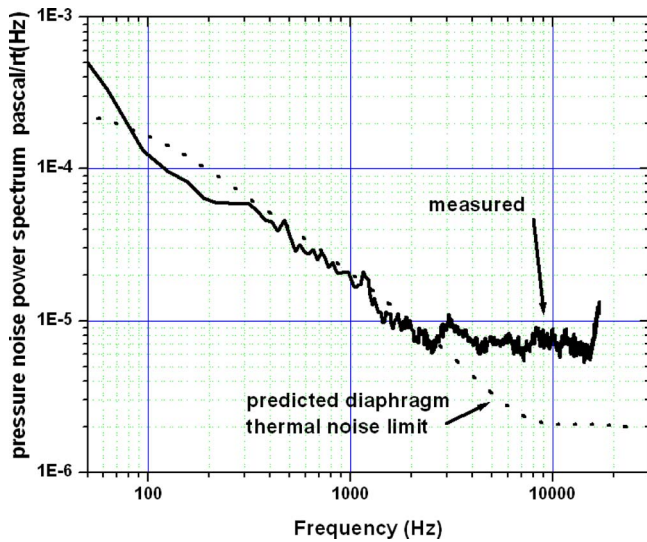
FIG. 13. (Color online) The equivalent sound input pressure-referred noise as predicted by Eq. (27) compared to the measured input pressure-referred noise. The measured results are obtained by dividing those of Fig. 12 by those given in Fig. 10. As in Fig. 12, the thermal noise limit was estimated by neglecting the contribution of electronic noise.

To compare the results obtained in the present study with those of commercially available hearing aid microphones, Eq. (31) has been evaluated to estimate the equivalent input noise of a differential sound sensor composed of two Knowles low-noise EM omnidirectional microphones. The noise floor of these omnidirectional microphones, $SPL_{oo}(\omega)$, obtained from Knowles.com, is shown in the figure along with the results of Eq. (31). It is assumed that the spacing between the microphones is $d_o = 10$ mm. The esti-
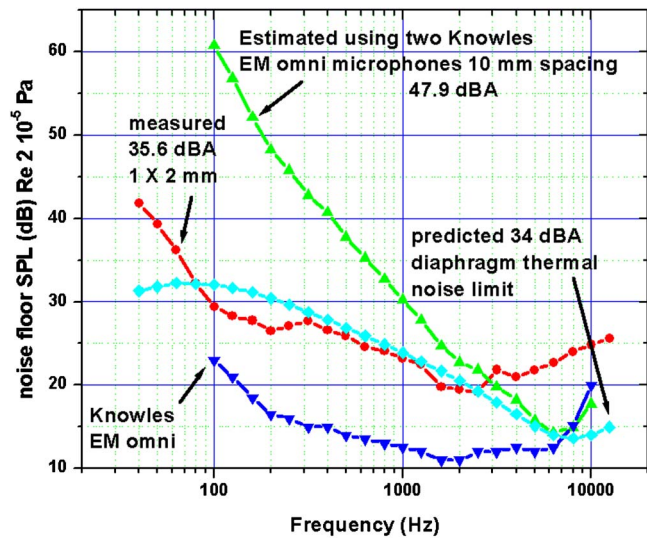

FIG. 14. (Color online) The one-third octave band levels of the narrowband input pressure-referred noise of Fig. 13. Equation (31) has been evaluated to estimate the equivalent input noise of a differential sound sensor composed of two Knowles low-noise EM omnidirectional microphones. The noise floor of these omnidirectional microphones, $SPL_{oo}(\omega)$, obtained from Knowles.com is shown in the figure along with the results of Eq. (31). It is assumed that the spacing between the microphones is $d_o = 10$ mm. The estimated noise of the differential sound sensor constructed by subtracting the output of the Knowles EM microphones is substantially higher than that of the differential microphone described here.

mated noise of the differential sound sensor constructed by subtracting the output of the Knowles EM microphones is substantially higher than that of the differential microphone described here. In the microphone developed here, one can roughly estimate the effective separation distance between the pressure sensors to be the distance between the centers of each side, separated by the axis of symmetry, which is half the diaphragm length, or 1 mm. It is important to note that the effective separation distance, d_o, of the omnidirectional microphones is ten times that of the microphone developed in the present study. As can be seen in Eq. (31), this factor of 10 gives the two microphone system a noise floor advantage of approximately 20 dB, yet its noise is substantially higher over much of the audible frequency range and its A-weighted noise floor of 47.9 dBA is more than 10 dB higher.

VI. CONCLUSIONS

The miniature differential microphone described in this paper is able to detect pressure gradients with minimal influence of microphone noise. This is accomplished through the use of a microphone diaphragm that rotates about a highly compliant central hinge due to an applied moment resulting from an incident sound wave. By minimizing the mass, stiffness, and passive damping in the diaphragm design, it is possible to achieve adequate sensitivity to sound and low thermal/mechanical noise. The use of a low-noise optical detection scheme has resulted in a design in which the total microphone noise is dominated by the diaphragm thermal/mechanical noise rather than noise in the electronic components over much of the audible frequency range.

APPENDIX: EMPIRICAL ESTIMATION OF DIFFERENTIAL MICROPHONE MECHANICAL PARAMETERS

The predictions of the response and noise performance through the analysis described in Sec. III above rely on knowledge of the effective mass, stiffness, and damping of the microphone diaphragm. For the rotational mode, these are I, k_t, and c_t in Eq. (4). These have been obtained by processing the measured response power spectra for the diaphragms due to a weakly stationary random acoustic excitation. The parameters are identified through a least squares approach where the mean square error in the model equation

J. Acoust. Soc. Am., Vol. 125, No. 4, April 2009

Miles *et al.*: Low noise differential microphone   2023

[Eq. (4)] is minimized (Su, 2005). The approach leads to a linear system of three normal equations for the three unknown parameters, I, k_t, and c_t. Power spectral density functions estimated from the measured random response are used to obtain the statistical information for construction of the normal equations. The empirical estimation process is outlined in this Appendix. It is shown that this procedure is essentially similar to the frequency domain method that is derived for deterministic signals presented in Raol *et al.* (2004), Napolitano *et al.* (2001), and Morelli (1999).

As discussed in Sec. III above, the mechanical system is modeled as a linear second order resonator, as described in Eq. (4). If the actual measured rotation of the diaphragm, $\theta(t)$, is entered into the equation, errors in the model will introduce an error in the net moment, $\epsilon(t)$, so that Eq. (4) becomes

$$\widetilde{I}\ddot{\theta}(t) + \widetilde{c}_t\dot{\theta}(t) = \widetilde{k}_t\theta(t) = M(t) + \epsilon(t). \tag{A1}$$

The mean squared error, $E[\epsilon^2(t)]$, where $E[\ ]$ is the expected value, is minimized by differentiating with respect to each unknown parameter,

$$\frac{\partial E[\epsilon^2(t)]}{\partial \widetilde{I}} = 0,$$

$$\frac{\partial E[\epsilon^2(t)]}{\partial \widetilde{c}_t} = 0,$$

$$\frac{\partial E[\epsilon^2(t)]}{\partial \widetilde{k}_t} = 0. \tag{A2}$$

Equations (A1) and (A2) lead to a system of equations for the unknown parameters that may be written in matrix form as

$$\begin{bmatrix} E[\ddot{\theta}^2] & E[\dot{\theta}\ddot{\theta}] & E[\theta\ddot{\theta}] \\ E[\ddot{\theta}\dot{\theta}] & E[\dot{\theta}^2] & E[\theta\dot{\theta}] \\ E[\ddot{\theta}\theta] & E[\dot{\theta}\theta] & E[\theta^2] \end{bmatrix} \begin{pmatrix} \widetilde{I} \\ \widetilde{c}_t \\ \widetilde{k}_t \end{pmatrix} = \begin{pmatrix} E[M\ddot{\theta}] \\ E[M\dot{\theta}] \\ E[M\theta] \end{pmatrix}. \tag{A3}$$

The expected values in Eq. (A3) may be expressed in terms of correlation functions $R_{\dot{\theta}\dot{\theta}}(\tau)$ and $R_{M\dot{\theta}}(\tau)$ when $\tau=0$. For weakly stationary signals, the correlation functions may be determined from the inverse Fourier transforms of the auto- and cross spectral density functions, $S_{\dot{\theta}\dot{\theta}}(\omega)$ and $S_{M\dot{\theta}}(\omega)$, by the *Weiner–Khinchine relations*.

$$E[\dot{\theta}(t)\dot{\theta}(t-\tau)] = R_{\dot{\theta}\dot{\theta}}(\tau) = \int_{-\infty}^{\infty} e^{\hat{j}\omega\tau} S_{\dot{\theta}\dot{\theta}}(\omega)d\omega,$$

$$E[M(t)\dot{\theta}(t-\tau)] = R_{M\dot{\theta}}(\tau) = \int_{-\infty}^{\infty} e^{\hat{j}\omega\tau} S_{M\dot{\theta}}(\omega)d\omega. \tag{A4}$$

The two-sided autospectral density function is real valued and an even function of frequency, and the two-sided cross spectral density function is complex with the real part an even function of frequency and the imaginary part an odd function of frequency (Bendat and Piersol, 1986; Lin, 1967). Therefore $S_{\dot{\theta}\dot{\theta}}(\omega)=S_{\dot{\theta}\dot{\theta}}(-\omega)$ and $S_{M\dot{\theta}}(-\omega)=S^*_{M\dot{\theta}}(\omega)$, where *

is the complex conjugate, and the expected values in Eq. (A3) are

$$E[\ddot{\theta}^2] = \int_{-\infty}^{\infty} \omega^2 S_{\dot{\theta}\dot{\theta}}(\omega)d\omega = 2\int_{0}^{\infty} \omega^2 S_{\dot{\theta}\dot{\theta}}(\omega)d\omega,$$

$$E[\dot{\theta}^2] = \int_{-\infty}^{\infty} S_{\dot{\theta}\dot{\theta}}(\omega)d\omega = 2\int_{0}^{\infty} S_{\dot{\theta}\dot{\theta}}(\omega)d\omega,$$

$$E[\theta^2] = \int_{-\infty}^{\infty} \frac{1}{\omega^2} S_{\dot{\theta}\dot{\theta}}(\omega)d\omega = 2\int_{0}^{\infty} \frac{1}{\omega^2} S_{\dot{\theta}\dot{\theta}}(\omega)d\omega,$$

$$E[\ddot{\theta}\theta] = E[\theta\ddot{\theta}] = -\int_{-\infty}^{\infty} S_{\dot{\theta}\dot{\theta}}(\omega)d\omega = -2\int_{0}^{\infty} S_{\dot{\theta}\dot{\theta}}(\omega)d\omega,$$

$$E[\ddot{\theta}\dot{\theta}] = E[\dot{\theta}\ddot{\theta}] = \int_{-\infty}^{\infty} \hat{j}\omega S_{\dot{\theta}\dot{\theta}}(\omega)d\omega = 0,$$

$$E[\dot{\theta}\theta] = E[\theta\dot{\theta}] = -\int_{-\infty}^{\infty} \frac{\hat{j}}{\omega} S_{\dot{\theta}\dot{\theta}}(\omega)d\omega = 0, \tag{A5}$$

and

$$E[M\ddot{\theta}] = \int_{-\infty}^{\infty} \hat{j}\omega S_{M\dot{\theta}}(\omega)d\omega = 2\int_{0}^{\infty} \Re[\hat{j}\omega S_{M\dot{\theta}}(\omega)]d\omega,$$

$$E[M\dot{\theta}] = \int_{-\infty}^{\infty} S_{M\dot{\theta}}(\omega)d\omega = 2\int_{0}^{\infty} \Re[S_{M\dot{\theta}}(\omega)]d\omega,$$

$$E[M\theta] = -\int_{-\infty}^{\infty} \frac{\hat{j}}{\omega} S_{M\dot{\theta}}(\omega)d\omega = -2\int_{0}^{\infty} \Re\left[\frac{\hat{j}}{\omega} S_{M\dot{\theta}}(\omega)\right]d\omega, \tag{A6}$$

where $\Re$ denotes the real part. Solving Eq. (A3) for the mechanical parameters gives

$$\widetilde{I} = \frac{E[\theta^2]E[M\ddot{\theta}] - E[\theta\ddot{\theta}]E[M\theta]}{E[\ddot{\theta}^2]E[\theta^2] - E[\theta\ddot{\theta}]^2},$$

$$\widetilde{c}_t = \frac{E[M\dot{\theta}]}{E[\dot{\theta}^2]},$$

$$\widetilde{k}_t = \frac{E[\ddot{\theta}^2]E[M\theta] - E[\ddot{\theta}\theta]E[M\ddot{\theta}]}{E[\ddot{\theta}^2]E[\theta^2] - E[\theta\ddot{\theta}]^2}. \tag{A7}$$

The finite Fourier transforms of the signals are

$$\dot{\Theta}(\omega,T) = \frac{1}{2\pi}\int_{-T}^{T} e^{-\hat{j}\omega t}\dot{\theta}(t)dt,$$

$$\mathcal{M}(\omega,T) = \frac{1}{2\pi}\int_{-T}^{T} e^{-\hat{j}\omega t}M(t)dt, \tag{A8}$$

which enables the calculation of the auto- and cross spectral densities,

$$S_{\dot{\theta}\dot{\theta}}(\omega) = \lim_{T\to\infty} \frac{\pi}{T} E[|\dot{\Theta}(\omega,T)|^2],$$

$$S_{M\dot{\theta}}(\omega) = \lim_{T\to\infty} \frac{\pi}{T} E[\mathcal{M}^*(\omega,T)\dot{\Theta}(\omega,T)]. \tag{A9}$$

When the signals are deterministic and their Fourier transforms exist, the identification procedure is the same as that described by Raol *et al.* (2004), Napolitano *et al.* (2001), and Morelli (1999). The Fourier transform can be applied to the governing equation and arranged as $\underline{Z} = [Y]\underline{\beta} + \underline{\varepsilon}$ for discrete data:

$$\begin{pmatrix} \mathcal{M}(\omega_1) \\ \mathcal{M}(\omega_2) \\ \vdots \\ \mathcal{M}(\omega_n) \end{pmatrix} = \begin{bmatrix} \ddot{\Theta}(\omega_1) & \dot{\Theta}(\omega_1) & \Theta(\omega_1) \\ \ddot{\Theta}(\omega_2) & \dot{\Theta}(\omega_2) & \Theta(\omega_2) \\ \vdots & \vdots & \vdots \\ \ddot{\Theta}(\omega_n) & \dot{\Theta}(\omega_n) & \Theta(\omega_n) \end{bmatrix} \begin{pmatrix} \tilde{I} \\ \tilde{c}_t \\ \tilde{k}_t \end{pmatrix} + \underline{\varepsilon}. \tag{A10}$$

The least squares solution for complex data is

$$\underline{\beta} = (\mathfrak{R}([Y]^{*T}[Y]))^{-1} \mathfrak{R}([Y]^{*T}\underline{Z}) \tag{A11}$$

and is the same solution as described in terms of the spectral densities when the signals are deterministic with $\ddot{\Theta}(\omega) = \hat{j}\omega\dot{\Theta}(\omega)$ and $\Theta(\omega) = -(\hat{j}/\omega)\dot{\Theta}(\omega)$.

1. Parameter estimation for the differential microphone diaphragm

The power spectra required in the above procedure were estimated from measured acoustic response of the microphones. Using a random excitation signal to drive a loudspeaker, a Doppler laser vibrometer (Polytec PSV-300H) was used to measure the out-of-plane velocity of the diaphragm and a probe microphone (Bruel and Kjaer Type 4182) measured the sound pressure at the diaphragm. Transfer functions of the velocity with respect to the sound pressure were estimated with a spectrum analyzer from averaged estimates of the auto- and cross power spectral densities. Two transfer functions for the diaphragm response were used for the mechanical parameter identification, $H_{p\dot{w}_1}(\omega)$ and $H_{p\dot{w}_2}(\omega)$, where $\dot{w}_1(t)$ and $\dot{w}_2(t)$ are the velocities at two points on opposite halves of the differential diaphragm separated by the pivot, and $p(t)$ is the sound pressure at the pivot. The spectral density functions in Eq. (A6) were estimated from $H_{p\dot{w}_1}(\omega)$, $H_{p\dot{w}_2}(\omega)$, and the sound pressure autospectral density $S_{pp}(\omega)$.

Assuming that the diaphragm is symmetric about the pivot axis, the rotation is approximated as $\theta = (w_1 - w_2)/(2d)$, and the driving moment is estimated from the sound pressure using the plane wave model, $M = -\dot{p}(t)\cos(\phi)I_a/c_0$. The auto- and cross spectral density functions that are needed in the identification procedure are related to the measured transfer functions by $S_{\dot{\theta}\dot{\theta}}(\omega) = |H_{p\dot{\theta}}(\omega)|^2 S_{pp}(\omega)$ and $S_{M\dot{\theta}}(\omega) = H_{pM}^*(\omega)H_{p\dot{\theta}}(\omega)S_{pp}(\omega)$, where $H_{p\dot{\theta}}(\omega) = (H_{p\dot{w}_1}(\omega) - H_{p\dot{w}_2}(\omega))/(2d)$, and $H_{pM}^*(\omega) = \hat{j}\omega\cos\phi I_A/c_0$. This gives

$$S_{\dot{\theta}\dot{\theta}}(\omega) = \left| \frac{H_{p\dot{w}_1}(\omega) - H_{p\dot{w}_2}(\omega)}{2d} \right|^2 S_{pp}(\omega),$$

$$S_{M\dot{\theta}}(\omega) = \frac{\hat{j}\omega\cos\phi I_A}{c_0}\left(\frac{H_{p\dot{w}_1}(\omega) - H_{p\dot{w}_2}(\omega)}{2d} \right) S_{pp}(\omega). \tag{A12}$$

The same procedure is used to estimate the parameters of the translational mode, governed by Eq. (19). The average diaphragm displacement is $X = (w_1 + w_2)/2$ and the average normal force due to the sound pressure is $F = pA$. The spectral density functions for the identification algorithm in this case are

$$S_{\dot{X}\dot{X}}(\omega) = \left| \frac{H_{p\dot{w}_1}(\omega) + H_{p\dot{w}_2}(\omega)}{2} \right|^2 S_{pp}(\omega),$$

$$S_{F\dot{X}}(\omega) = \frac{A(H_{p\dot{w}_1}(\omega) + H_{p\dot{w}_2}(\omega))}{2} S_{pp}(\omega). \tag{A13}$$

The integrals of the spectral density functions for the expected values are approximated by summation over a user selected frequency range, where the mode in question is dominant, and where data quality is good, as verified by coherence squared functions.

Akcakaya, M., and Nehorai, A. (**2008**). "Performance analysis of the *Ormia ochracea's* coupled ears," J. Acoust. Soc. Am. **124**, 2100–2105.

Amlani, A. M., Rakerd, B., and Punch, J. L. (**2006**). "Speech-clarity judgments of hearing-aid-processed speech in noise: Differing polar patterns and acoustic environments," Int. J. Audiol. **45**, 319–330.

Ando, S. (**1995**). "An intelligent three-dimensional vision sensor with ears," Sens. Mater. **7**, 213–231.

Ando, S., Ono, N., and Fujita, Y. (**2007**). "Partial differential equation-based algorithm of sound source localization with finest granularity in both time and frequency," in *Proceedings of International Conference Networked Sensing Systems (INSS2007)*, pp. 229–234.

Bendat, J. S., and Piersol, A. G. (**1986**). *Random Data Analysis and Measurement Procedures* (Wiley, New York).

Beranek, L. L. (**1954**). *Acoustics* (Acoustical Society of America, Woodbury, NY).

Blamey, P. J., Fiket, H. J., and Steele, B. R. (**2006**). "Improving speech intelligibility in background noise with an adaptive directional microphone," J. Am. Acad. Audiol **17**, 519–530.

Blumlein, A. D. (**1931**). "Directional effect in sound systems," British Patent No. 394,325.

Chen, Z., and Yu, M. (**2008**). "Biology-inspired acoustic sensors for sound source localization," in *Proceedings of the SPIE Smart Structures and Materials & Nondestructive Evaluation and Health Monitoring, 15th Annual International Symposium*, San Diego, CA, Vol. **6932–108**.

Cui, W., Jones, S. A., Miles, R. N., Degertekin, F. L., Hall, N., and Bicen, B. (**2006**). "Optical sensing in a directional MEMS microphone inspired by the ears of the parasitoid fly, *Ormia ochracea*," in *19th IEEE Conference on Micro Electro Mechanical Systems (MEMS 2006)*, Istanbul, Turkey.

Freidlander, B. (**1984**). "On the Cramer–Rao bound for time delay and Doppler estimation," IEEE Trans. Inf. Theory **IT-30**, 575–580.

Gabrielson, T. (**1993**). "Mechanical-thermal noise in micromachined acoustic and vibration sensors," IEEE Trans. Electron Devices **40**, 903–909.

Gerzon, M. A. (**1994**). "Applications of Blumlein shuffling to stereo microphone techniques," J. Audio Eng. Soc. **42**, 435–453.

Gibbons, C., and Miles, R. N. (**2000**). "Design of a biomimetic directional microphone diaphragm," in *Proceedings of the International Mechanical Engineering Congress and Exposition*, Orlando, FL.

Hall, N. A., and Degertekin, F. L. (**2002**). "An integrated optical interferometric detection method for micromachined capacitive acoustic transducers," Appl. Phys. Lett. **80**, 3859–3861.

Hall, N. A., Bicen, B., Lee, W., Jeelani, K., Qureshi, S., Okandan, M., and

Degertekin, F. L. (**2005**). "Micromachined microphones with diffraction-based optical displacement detection," J. Acoust. Soc. Am. **118**, 3000–3009.

Hall, N. A., Okandan, M., Littrell, R., Bicen, B., and Degertekin, F. L. (**2007**). "Micromachined optical microphone structures with low thermal-mechanical noise levels," J. Acoust. Soc. Am. **122**, 2031–2037.

Homentcovschi, D., and Miles, R. N. (**2004**). "Modeling of viscous damping of perforated planar microstructures. Applications in acoustics," J. Acoust. Soc. Am. **116**, 2939–2947.

Homentcovschi, D., and Miles, R. N. (**2005**). "Viscous damping of perforated planar micromechanical structures," Sens. Actuators, A **119**, 544–552.

Hornsby, B. W., and Ricketts, T. A. (**2007**). "Effects of noise source configuration on directional benefit using symmetric and asymmetric directional hearing aid fittings," Ear Hear. **28**, 177–186.

Lee, W., Hall, N. A., Zhou, Z., and Degertekin, F. L. (**2004**). "Fabrication and characterization of a micromachined acoustic sensor with integrated optical readout," IEEE J. Sel. Top. Quantum Electron. **10**, 643–651.

Lin, Y. K. (**1967**). *Probabilistic Theory of Structural Dynamics* (Robert E. Krieger, Malabar, FL).

Lockwood, M. E., and Jones, D. L. (**2006**). "Beamformer performance with acoustic vector sensors in air," J. Acoust. Soc. Am. **119**, 608–619.

Mason, A., Oshinsky, M., and Hoy, R. R. (**2001**). "Hyperacute directional hearing in a microscale auditory system," Nature (London) **410**, 686–690.

Miles, R. N. (**2008**). "Low-noise directional hearing aid microphone using optical sensing with electronic feedback," National Institutes of Health Grant No. 1R01DC009429-01.

Miles, R. N., and Degertekin, F. L. (**2007**). "Optical sensing in a directional MEMS microphone," U.S. Patent No. US2007/0165896 A1.

Miles, R. N., and Hoy, R. R. (**2006**). "The development of a biologically-inspired directional microphone for hearing aids," Audiol. Neuro-Otol. **11**, 86–94.

Miles, R. N., Cui, W., Miller, R. A., Su, Q., Tan, L., and Weinstein, M. G. (**2002**). "Response of a biologically inspired MEMS differential microphone diaphragm," in *Proceedings of the SPIE AeroSense 2000*, Orlando, FL, Paper No. 4743-15.

Miles, R. N., Robert, D., and Hoy, R. R. (**1995**). "Mechanically coupled ears for directional hearing in the parasitoid fly *Ormia ochracea*," J. Acoust. Soc. Am. **98**, 3059–3070.

Miles, R. N., Sundermurthy, S., Gibbons, C., Hoy, R., and Robert, D. (**2004**). "Differential Microphone," U.S. Patent No. 6,788,796 B1.

Miles, R. N., Tieu, T. D., Robert, D., and Hoy, R. R. (**1997**). "A mechanical analysis of the novel ear of the parasitoid fly *Ormia ochracea*," in *Proceedings: Diversity in Auditory Mechanics*, edited by E. R. Lewis, G. R. Long, R. F. Lion, P. M. Narins, C. R. Steele, and E. Hecht-Poinar (World Scientific, Singapore), pp. 18–24.

Mohan, S., Lockwood, M. E., Kramer, M. L., and Jones, D. L. (**2008**). "Localization of multiple acoustic sources with small arrays using a coherence test," J. Acoust. Soc. Am. **123**, 2136–2147.

Morelli, E. A. (**1999**). "Real-time parameter estimation in the frequency domain," AIAA-99-4043.

Napolitano, M. R., Song, Y., and Seanor, B. (**2001**). "On-line parameter estimation for restructurable flight control systems," Aircraft Design. **4**, 19–50.

Olson, H. F. (**1947**). *Elements of Acoustical Engineering* (D. Van Nostrand Co., Inc., New York), Chap. 8.3.

Ono, N., Arita, T., Senjo, Y., and Ando, S. (**2005**). "Directivity Steering Principle for Biomimicry Silicon Microphone," in *13th International Conference on Solid-State Sensors, Actuators and Microsystems Transducers '05*, Seoul, Korea.

Oshinsky, M. L. (**1998**). "Physiological correlates of sound localization in a parasitoid fly, *Ormia ochracea*," Ph.D. thesis, Cornell University, Ithaca, NY.

Raol, J. R., Girija, G., and Singh, J. (**2004**). *Modeling and Parameter Estimation of Dynamic Systems*, The Institution of Electrical Engineers, London.

Ricketts, T., Henry, P., and Gnewikow, D. (**2003**). "Full time directional versus user selectable microphone modes in hearing aids," Ear Hear. **24**, 424–439.

Saito, A., Ono, N., and Ando, S. (**2002**). "Micro gimbal diaphragm for sound source localization with mimicking Ormia Ochracea," in *Proceedings of the 41st SICE Annual Conference Society for Instrument and Control Engineers (SICE)*.

Stanacevic, M., and Cauwenberghs, G. (**2005**). "Micropower gradient flow acoustic localizer," IEEE Trans. Circuits Syst., I: Regul. Pap. **52**, 2148–2157.

Su, Q. T. (**2005**). "Measurement and characterization of miniature silicon microphone diaphragms," Ph.D. thesis, State University of New York Binghamton, Binghamton, NY.

Sung, P.-H., Chen, J.-Y., Yen, K.-H., and Wu, C.-Y. (**2007**). "CMOS compatible directional microphone," in Microsystems, Packaging, Assembly and Circuits Technology, IMPACT 2007, Vols. **1–3**, pp. 149–152.

Thompson, S. C., LoPresti, J. L., Ring, E. M., Nepomuceno, H. G., Beard, J. J., Ballad, W. J., and Carlson, E. V. (**2002**). "Noise in miniature microphones," J. Acoust. Soc. Am. **111**, 861–886.

Walden, B. E., Surr, R. K., Cord, M. T., and Dyrlund, O. (**2004**). "Predicting hearing aid microphone preference in everyday listening," J. Am. Acad. Audiol **15**, 365–396.

Yoo, K., Yeh, J.-L. A., Tien, N. C., Gibbons, C., Su, Q., and Miles, R. N. (**2002**). "Fabrication of biomimetic 3-D structured diaphragms," Sens. Actuators, A **97–98**, 448–456.